Available online at www.sciencedirect.com
SCIENCE DIRECT®
Journal of Power Sources 137 (2004) 228–238
JOURNAL OF POWER SOURCES
www.elsevier.com/locate/jpowsour

A one dimensional model of a methanol fuel cell anode

K. Scott*, P. Argyropoulos

Department of Chemical and Process Engineering, Merz Court, University of Newcastle, Newcastle upon Tyne NE1 7RU, UK

Received 5 June 2003; received in revised form 21 January 2004; accepted 22 March 2004
Available online11 September 2004

Abstract

A model of a direct methanol fuel cell anode is presented which considers electrocatalysts to have a distribution of over potential and current density in the structure. The model is applicable to an anode based on a metal mesh supported electrocatalysts structure. Methanol oxidation is described by dual site mechanisms involving adsorbed CO and OH intermediates. The model is used to predict the electrode potential–current density behaviour of the anode. The concentration of methanol is shown to influence overall electrode polarisation characteristics and critically the selection of the mechanism for methanol oxidation has a major impact in this respect. The model gives good correspondence with experimentally observed cell polarisation behaviour.

Keywords: Direct methanol fuel cell; Polymer electrolyte; Proton-exchange; Model; Anode catalyst

1. Introduction

Proton-exchange membrane (PEM) fuel cells are alternative power sources for stationary and mobile applications and electric vehicles. Methanol is a liquid fuel that has substantial electroactivity and can be oxidised directly to carbon dioxide and water on catalytically active anodes in a direct methanol fuel cell (DMFC):

$$CH_3OH + H_2O \rightarrow CO_2 + 6H^+ + 6e^- \quad (1)$$

The direct methanol fuel cell, based on a solid polymer electrolyte (SPE) in the form of a proton conducting membrane, has the attraction of no liquid acidic or alkaline electrolyte. The structure of the DMFC is a composite of two porous electrocatalytic electrodes on either side of a solid polymer electrolyte membrane. In the DMFC, platinum alone is not a sufficiently active methanol oxidation electrocatalyst and the promotion of methanol oxidation has been actively studied. Significant results have been achieved with the use of binary catalysts, notably Pt–Ru. With these catalysts the second metal forms a surface oxide used in the potential range for methanol oxidation [1]. The mechanism of methanol oxidation can be represented as [2]:

$$CH_3OH \rightarrow CO_{ads} + 4H^+ + 4e^-,$$
$$H_2O \rightarrow OH_{ads} + H^+ + e^-,$$
$$CO_{ads} + 2OH_{ads} \rightarrow CO_2 + H_2O \quad (2)$$

It is generally thought that the rate controlling step is surface reaction between CO_{ads} and OH_{ads}. It has been proposed that methanol and hydroxyl groups are adsorbed on different parts of the surface on carbon supported platinum. However despite significant research on methanol oxidation, the mechanism is not fully known and the adsorption of the various reactive intermediates may involve a combination of single site and dual site processes [3].

Recent developments in electrode fabrication techniques and better cell designs have brought dramatic improvements in cell performance in small-scale DMFCs [4–14]. An essential condition for the high performance of a DMFC is the use of relatively low methanol concentrations. At concentrations higher than approximately 2 mol dm^{-3}, the cell voltage declines significantly due to permeation of methanol through the SPE (Nafion®) membrane, i.e. methanol crossover. This permeation results in a mixed potential at the cathode with a significant loss in oxygen reduction performance and also poor fuel utilisation. Thus an important area to improve the DMFC performance is in polymer membrane electrolytes to reduce methanol crossover.

Previous models of the DMFC have been few. Verbrugge described a simple diffusion model of methanol through a PEM, assuming dilute solution theory [15]. Validation of

* Corresponding author. Tel.: +44-191-222-8771; fax: +44-191-222-5292.
E-mail address: k.scott@ncl.ac.uk (K. Scott).

0378-7753/$ – see front matter © 2004 Elsevier B.V. All rights reserved.
doi:10.1016/j.jpowsour.2004.03.049

the model with experimental data showed that the diffusion rate of methanol through the membrane was nearly as fast as through water. A second model, across a PEM has been used to explain observed experimental data for a vapour feed DMFC [16]. This model has been extended to include a one dimensional model of the potential distribution and concentration distribution of methanol in the anode electrocatalyst layer for a vapour feed system [5,17]. The model gives good agreement with experimental data except under conditions where mass transport becomes rate limiting. Baxter et al. [18] have presented a model of the DMFC anode which is considered to be a porous electrode consisting of an electronically conducting catalyst structure that is thinly coated with an ion selective polymer electrolyte. The pores of the electrode are filled with aqueous methanol solution in which all species undergo mass to transport. Mass transfer in the anode is defined in terms of a pseudo-mass-transport coefficient. The model is however not validated against experimental data and does not consider mass transport of species in other regions of the electrode assembly.

A two-dimensional mathematical modelling of an SPE–DMFC, both for vapour and liquid-feed configurations, has been presented by Kulikovsky et al. [19,20] employing Stefan–Maxwell molecular diffusion and Knüdsen diffusion mechanism, while neglecting the methanol crossover component. Sundmacher et al. [21] studied both the static and the dynamic response of an SPE–DMFC and showed that methanol crossover in the cell can be reduced by pulsed methanol feed. Wang et al. [22,23] have presented a two-dimensional and biphasic, multicomponent mathematical model for an SPE–DMFC. The model includes the crossover effects due to diffusion, convection and electro-osmosis and the resultant mixed potential due to methanol oxidation at the cathode. Although the transport in the porous media is quite accurately treated in the model, the catalyst layer has been considered to be infinitesimally thin excluding the polarisation effects arising from mass transport of reactants within the layer. Quite recently, Meyer and Newman [24,25] have presented modelling and data analysis of transport phenomena in an SPE–DMFC. In contrast to most of the earlier models, which employ a simple Butler–Völmer (BV) relationship for describing the electrode-kinetics for methanol oxidation at the anode, the model due to Meyer and Newman follows the reaction mechanism proposed by Gaisteiger et al. [26].

In this paper we present a simple model of a methanol oxidation anode in which a distribution in overpotential occurs in the structure. The model is applicable to a new type of anode for the DMFC currently being investigated in our laboratories.

2. Kinetics of methanol oxidation

The following reaction mechanism is based on a simplification of a more general model of methanol oxidation [27]. The mechanism is a reasonable approximation in view of the great difficulties in determining kinetic parameters for the multi-reaction paths of methanol oxidation:

$$\mathrm{CH_3OH} \underset{k_1^1}{\overset{k_1}{\Leftrightarrow}} \mathrm{CH_3OH_{ads}} \tag{3}$$

$$\mathrm{CH_3OH_{ads}} \underset{k_2^1}{\overset{k_2}{\Leftrightarrow}} \mathrm{CO_{ad}} + 4\mathrm{H^+} + 4\mathrm{e^-} \tag{4}$$

$$\mathrm{H_2O} \underset{k_3^1}{\overset{k_3}{\Leftrightarrow}} \mathrm{OH_{ads}} + \mathrm{H^+} + \mathrm{e^-} \tag{5}$$

The rate determining step (i.e. slow process) is taken as

$$\mathrm{CO_{ads}} + 2\mathrm{OH_{ads}} \overset{k_4}{\rightarrow} \mathrm{CO_2} + \mathrm{H_2O} \tag{6}$$

This will apply until conditions are such that mass-transport limitations of methanol occur, typically at high current densities which are not of practical interest.

We assume that steps (3)–(5) are in equilibrium. Step (5) principally includes adsorption on Ru sites, whereas, steps (3) and (4) involve adsorption primarily onto platinum. The latter condition is valid as it is known that Ru is a poor electrocatalyst for methanol oxidation.

From equilibrium of reactions (3)–(5) we obtain

$$k_1 C_\mathrm{M} (1 - \theta_\mathrm{M} - \theta_\mathrm{CO}) = k_1 \theta_\mathrm{M} \tag{7}$$

where θ_M and θ_CO refers to the fractional coverage of methanol and CO, respectively.

$$k_2 \theta_\mathrm{M} = k_2^1 \theta_\mathrm{CO} \tag{8}$$

where

$$k_2 = k_2^0 \exp\left[\frac{(1-\beta_2)F}{R}E\right], \qquad k_2^1 = k_2^{01} \exp\left[-\alpha_2 F \frac{E}{RT}\right]$$

noting that we do not assume symmetry of electrochemical reaction and

$$k_3(1 - \theta_\mathrm{OH}) = k_3^1 \theta_\mathrm{OH} \tag{9}$$

where

$$k_3 = k_{30} \exp\left[(1-\beta_3)F\frac{E}{RT}\right],$$

$$k_3^1 = k_{30}^1 \exp\left[-\beta_3 F \frac{E}{RT}\right]$$

The activity of water is assumed to be 1.0.

Eqs. (7)–(9) combine to give:

$$\theta_\mathrm{CO} = \frac{K_2 K_1 C_\mathrm{M}}{(1 + K_1, C_\mathrm{M}(1 + K_2))} \tag{10}$$

$$\theta_\mathrm{OH} = \frac{K_3}{1 + K_3} \tag{11}$$

Now $K_2 \gg 1$ therefore Eq. (10) becomes

$$\theta_\mathrm{CO} = \frac{K_2 K_1 C_\mathrm{M}}{1 + K_1 K_2 C_\mathrm{M}} \tag{12}$$

where $K_1 = k_1/k_1^1$, $K_2 = k_2/k_2^1$, $K_3 = k_3/k_3^1$.

The rate of reaction (6) is therefore

$$r_6 = \frac{j}{6F} = k_4\theta_{OH}^2\theta_{CO} = k_4\left(\frac{K_3}{1+K_3}\right)^2\frac{K_2K_1C_M}{1+K_2K_1C_M} \quad (13)$$

We define the potential E in terms of overpotential η and the open-circuit potential U_o, i.e.

$$E = \eta + U_o \quad (14)$$

The reaction current density is therefore written as

$$j = \frac{k_{10}C_M\exp(((1-\beta_2+\alpha_2)/RT)F\eta)}{1+C_Mk_{20}\exp(((1-\beta_2+\alpha_2)/RT)F\eta)} \quad (15)$$

where

$$k_{10} = 6Fk_4\frac{k_2^0}{k_2^{01}}\frac{k_1}{k_1^1}\exp(1-\beta_2+\alpha_2)\frac{FU_o}{RT}$$

and $$k_{20} = \frac{k_{10}}{k_4 6F}$$

and noting $K_3 \gg 1$ for most practical fuel cell conditions.

With the substitution $\beta = (1-\beta_2+\alpha_2)(F/RT)$ we write Eq. (15) in a more convenient form as

$$j = \frac{6Fk_{10}C_M\,e^{\beta\eta}}{1+k_{20}C_M\,e^{\beta\eta}} \quad (16)$$

or

$$j = \frac{C_M}{[(1/6Fk_{10}\exp(\beta\eta)) + (k_{20}C_M/6Fk_{10})]}$$

Fig. 1 shows experimental data for the oxidation of methanol at a fuel cell anode at temperatures of 60 and 90 °C [28]. The data clearly show that methanol oxidation exhibits a limiting current density which may be due to mass transport or to the mechanism of methanol oxidation in which adsorption is a major factor. This behaviour is further discussed later. Plotted on the figure is a Tafel approximation of the data based on fitting the following equation at low current densities:

$$j = 6Fk_{10}C_M\exp(\beta\eta) \quad (17)$$

Clearly over the lower range of potentials the fit to the Tafel type equation is reasonable.

Fig. 2 shows experimental data for methanol oxidation obtained at 60 and 90 °C, and the fit of the data to Eq. (16). The fit has been achieved by using the value of the limiting current density, as defined from Eq. (16) as $j = k_{10}/k_{20}$, to determine k_{20} and then using the data obtained for the Tafel correlation for k_{20} and β. The data at the two temperatures has been correlated using two values of β and two values of the constant k_{20}. The model shows reasonable agreement with experimental data.

Fig. 3 shows the effect of changing the value of β on the correlation of the experimental data aimed at improving the fit in the range of current densities >1000 A m^{-2}. This is done by reducing the values of the constants k_{10} and k_{20}, when the value of β was reduced. Although a reasonable agreement with data is achieved at higher current densities, in this case the fit to the data at low current densities is not good.

Fig. 4 shows the effect of varying the ratio of k_{20}/k_{10} on the anode polarisation and compares the resulted fits with experimental data and the results based on the Tafel approximation of Eq. (16). The term k_{20}/k_{10} actually relates to the rate coefficient for reaction step (6) in the mechanism and the smaller its value the greater is the rate of this step. Hence, as expected, with a relatively fast reaction rate, between the surface species, methanol oxidation overpotential behaviour becomes more favourable, i.e. polarisation is lower at a given current density, and the limiting currents are higher.

Fig. 5 shows the effect of methanol concentration on anode polarisation. At a fixed potential the overpotential

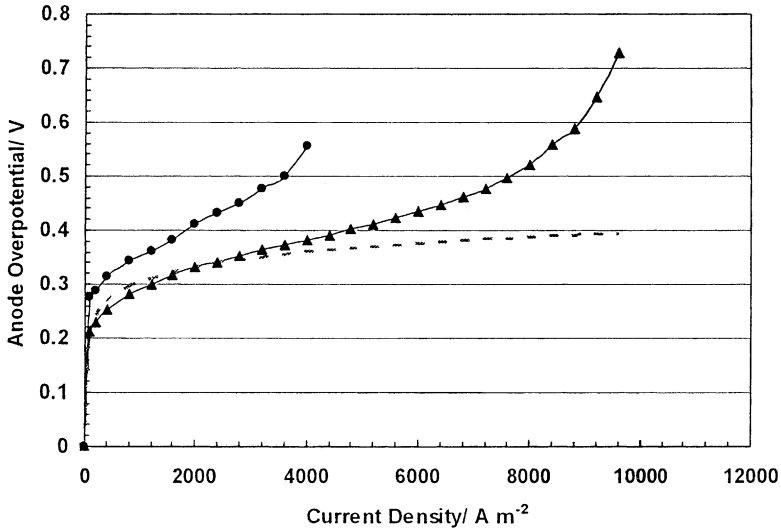

Fig. 1. Experimental data for the oxidation of methanol at a fuel cell anode at a temperature of: (▲) 90 °C and (●) 60 °C [28].

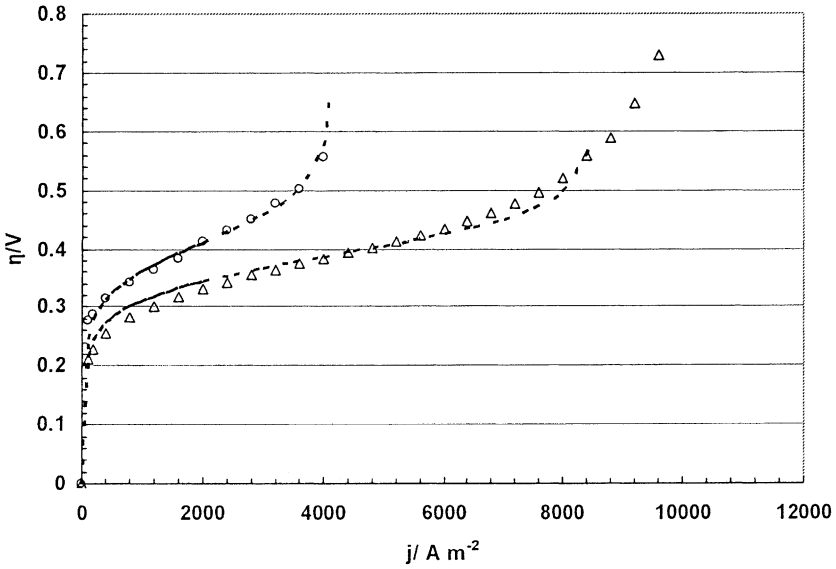

Fig. 2. Experimental data for methanol oxidation obtained at 60 and 90 °C [28] and the fit of the data to Eq. (16): (90 °C, △) $k_{10} = 8.64 \times 10^{-10}$, $k_{20} = 5.83 \times 10^{-8}$, $\beta = 24.91$; (60 °C, ○) $k_{10} = 8.64 \times 10^{-10}$, $k_{20} = 1.21 \times 10^{-7}$, $\beta = 21.84$. $C_M = 1000\,\mathrm{mol\,m^{-3}}$.

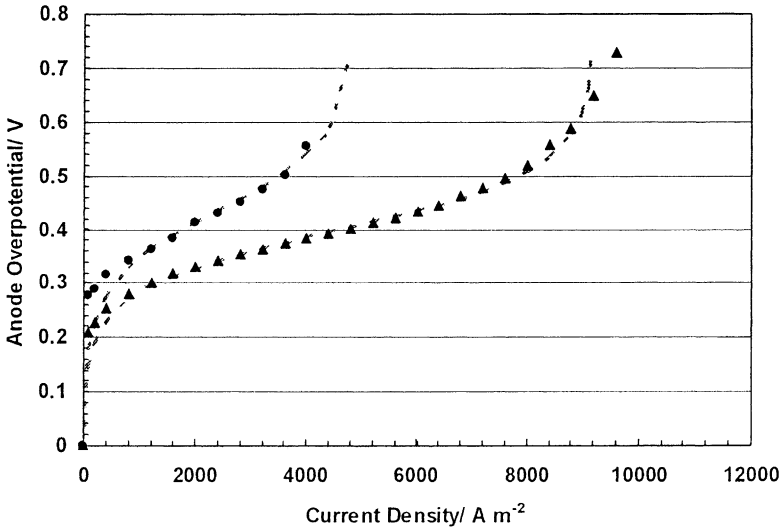

Fig. 3. The effect of β on the correlation of experimental data using model equation (16) for methanol oxidation: (90 °C, ▲) $k_{10} = 1.22 \times 10^{-8}$, $\beta = 17.92$, $k_{20} = 7.68 \times 10^{-7}$; (60 °C, ●) $k_{10} = 1.22 \times 10^{-8}$, $\beta = 14.95$, $k_{20} = 1.45 \times 10^{-6}$.

decreases as the methanol concentration is increased. The data exhibits the characteristic that, at high potentials, a common limiting current is achieved at all concentrations of methanol. This behaviour in contrary to that reported in a number of studies of methanol oxidation and may be a result of the influence of mass-transport limitations in practical fuel cell anodes or to limitations in the model above. We address this latter point first.

2.1. The Gasteiger mechanism

An alternative mechanism for methanol oxidation [26] is similar to that proposed above

$$CH_3OH \underset{k_1^1}{\overset{k_1}{\rightarrow}} CH_3OH_{ads} \tag{18}$$

$$CH_3OH_{ads} \underset{k_2^1}{\overset{k_2}{\Leftrightarrow}} CO_{ad} + 4H^+ + 4e^- \tag{19}$$

$$H_2O \underset{k_3^1}{\overset{k_3}{\Leftrightarrow}} OH_{ads} + H^+ + e^- \tag{20}$$

The rate determining step (i.e. slow process) is taken as

$$CO_{ads} + 2OH_{ads} \overset{k_4}{\rightarrow} CO_2 + H_2O \tag{21}$$

except, when the concentration of methanol is small.

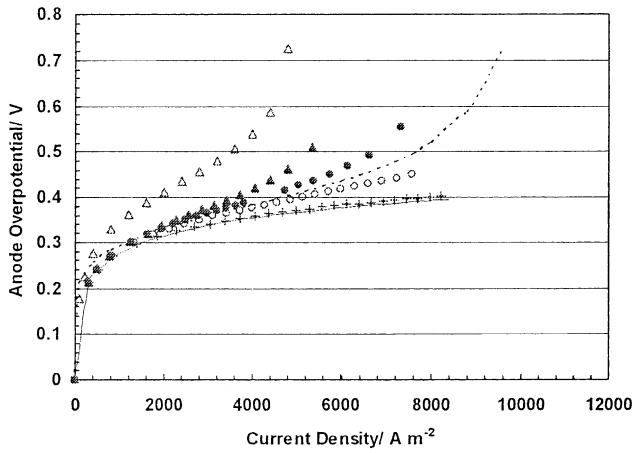

Fig. 4. The effect of varying the ratio of k_{20}/k_{10}: (△) 100, (▲) 75, (○) 50, (●) 25, (+) 10. Dotted line: experimental data; continuous line: Tafel equation.

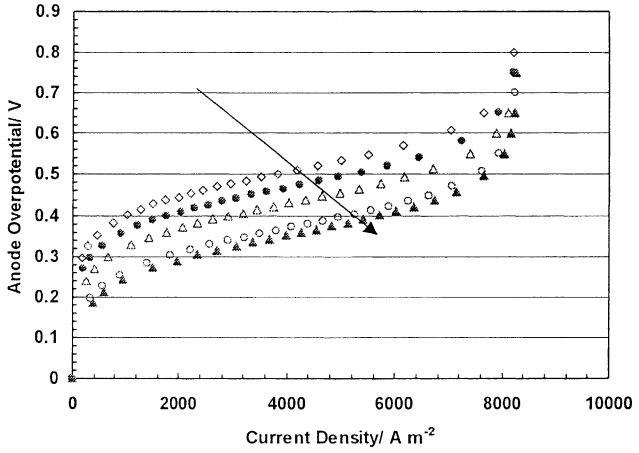

Fig. 5. The effect of methanol concentration on the polarisation curve for the methanol fuel cell anode: (◇) 125, (●) 250, (△) 500, (○) 1500, (▲) 2000. $k_{20}/k_{10} = 70$. 90 °C. $k_{10} = 1.22 \times 10^{-8}$, $\beta = 17.92$, $k_{20} = 7.68 \times 10^{-7}$.

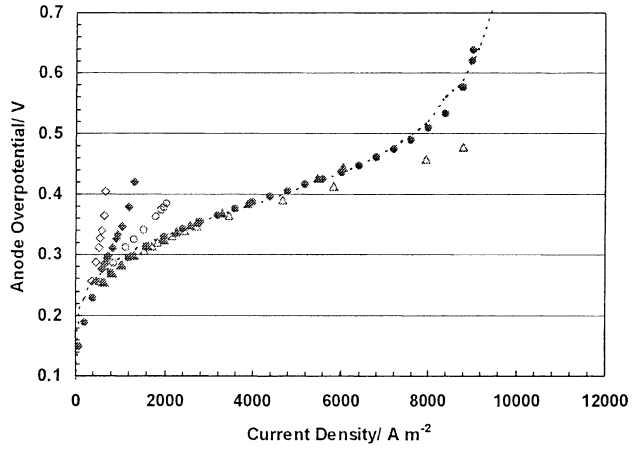

Fig. 7. The effect of methanol concentration on the methanol oxidation polarisation characteristics: (◇) 0.125, (▲) 0.25, (○) 0.5, (●) 1.0, (◆) 1.5, (△) 2.0. 90 °C. $k_{10} = 1.22\text{E}{-}05$, $\beta = 17.91819$, $k_{20} = 0.768343$.

The model assumes that reaction steps (19) and (20) are in equilibrium and produces the overall expression:

$$j = \frac{6Fk_{10}C_{\mathrm{M}} \exp(\beta\eta)}{C_{\mathrm{M}} + k_{20} \exp(\beta\eta)} \tag{22}$$

where the terms k_{10} and k_{20} are different group terms to those in Eq. (16).

Fig. 6 shows the fit of model equation (22) to experimental data at temperatures of 60 and 90 °C. With the data available, this model also gives a good prediction of methanol oxidation polarisation characteristics. However Eq. (22) predicts (Fig. 7) different behaviour to Eq. (15), i.e. at low overpotential, the current density at a fixed overpotential is independent of C_{M} and at high overpotential j is proportional to C_{M}. There is a body of literature data that agrees partly with the latter characteristics. However there is less evidence, in terms of reported data, that is in accord with the invariance of methanol oxidation currents with methanol concentration, at low overpotentials.

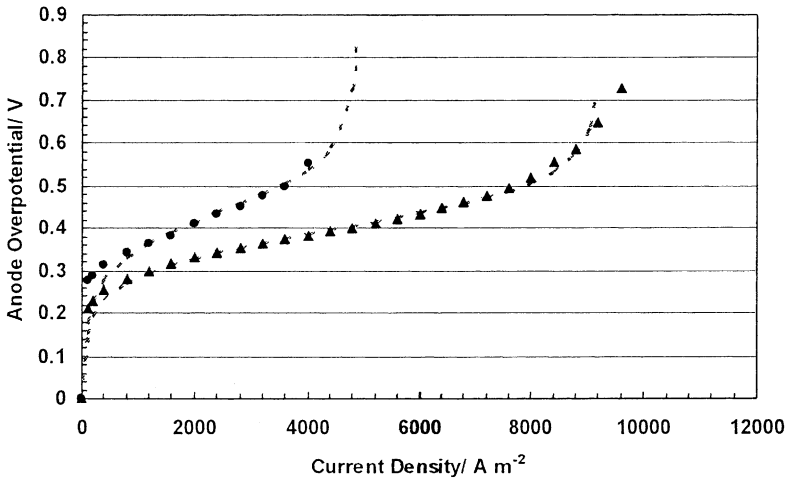

Fig. 6. The comparison of experimental methanol oxidation data with the model based on the mechanism of Gasteiger: (90 °C, ▲) $k_{10} = 1.22 \times 10^{-5}$, $\beta = 17.92$, $k_{20} = 0.77$; (60 °C, ●) $k_{10} = 1.22 \times 10^{-5}$, $\beta = 14.95$, $k_{20} = 1.45$.

2.2. Implications of diffusion mass transport

The basic difference between the two models of the mechanism for methanol oxidation presented above is that in one case the adsorption of methanol species is taken as an equilibrium process (Frelink) and in the other case it is not (Gasteiger). The consequence of this difference is that a limit to the current density for methanol oxidation arises which in one case is independent of methanol concentration and in the other case it is approximately proportional to the methanol concentration. In previous experimental work [7,29] with fuel cell electrodes, limiting currents have been produced which increase with an increase in methanol concentration. These limiting currents have been interpreted as either due to mass-transport limitations in the fuel cell electrode [29] or as a consequence of the mechanism of methanol oxidation [2]. However, with much of the published data for fuel cell electrodes, based on carbon supported catalysts, it is not readily possible to differentiate the major factor which causes a limiting current. A factor in the DMFC is that of the gas evolution in the porous structure which will have a controlling influence on diffusion and convective mass transport. Essentially as the methanol concentration is increased, then any increase in limiting current may be a consequence of the greater rate of carbon dioxide evolution. Furthermore it is also possible that both kinetic (mechanistic) and mass-transport limitations may occur at similar overpotentials or current densities. For example, if we consider the limit of the Gasteiger model at higher overpotentials, then we see that

$$j \approx \frac{6Fk_{10}C_{\mathrm{M}}}{k_{20}} \tag{23}$$

where C_{M} is the concentration of methanol at the catalyst surface.

For a simple mass-transport model, based on a mass-transport coefficient k_{L}, the current density can be expressed as

$$j = 6Fk_{\mathrm{L}}(C_{\mathrm{Mb}} - C_{\mathrm{M}}) \tag{24}$$

where C_{Mb} is the bulk concentration of methanol.

Combining these two equations we obtain

$$j = \frac{6Fk_{\mathrm{L}}C_{\mathrm{Mb}}}{(1/k_{\mathrm{L}}) + (k_{20}/k_{10})} \tag{25}$$

The limiting current is proportional to the methanol concentration and its magnitude depends upon the combined values of the kinetic and mass-transport coefficients.

To determine whether the limiting current is a result of the reaction mechanism, requires a study of methanol oxidation under well defined and controllable mass-transport conditions, for example using a rotating disc electrode.

Furthermore, the majority of methanol fuel cell anodes are high surface area materials which will exhibit a current distribution normal to the direction of current flow. This factor will also have an influence on the methanol anode polarisation behaviour as is the subject of the following section.

3. Current distribution model

We adopt a model for the catalyst structure in which the supported catalyst is electronically in contact with the current collector e.g. carbon and ionically in contact with the membrane through a Nafion bonding layer. The concentration of methanol within the pores is assumed uniform.

The region from $x = 0$ to $x = 1$ is the catalyst region in which the concentration of reactant is assumed constant (Fig. 8). This situation applies to a system with negligible mass-transport resistance in the pores or when an approximate well mixed condition applies. This applies to an-

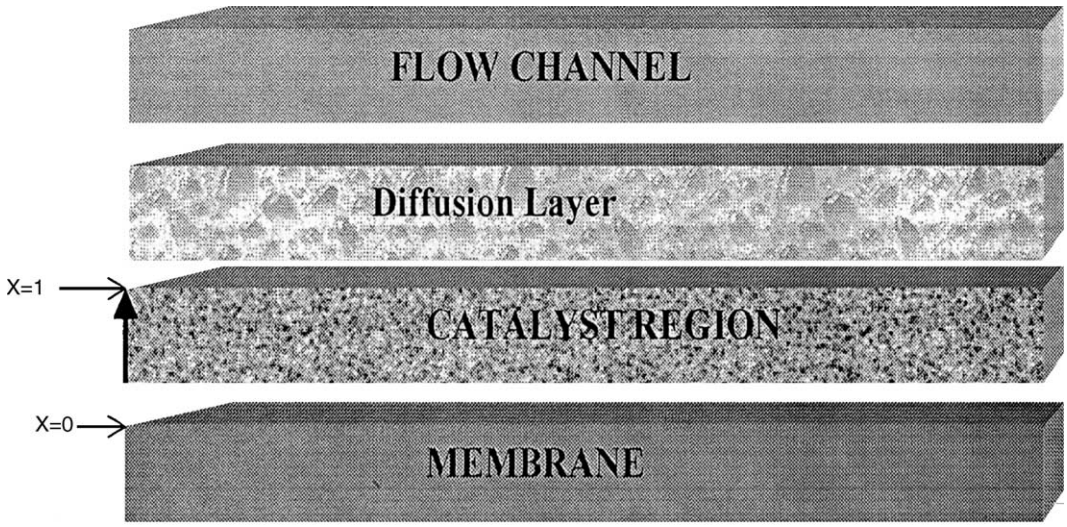

Fig. 8. Schematic model of methanol fuel cell anode.

odes which are based on Ti mesh supported electrocatalysts [30].

Applying Ohm's law to proton and electron motion in the carbon/catalyst region and ionomer region covering the catalyst gives

$$-\sigma\frac{\mathrm{d}\phi_\mathrm{m}}{\mathrm{d}x} = j \tag{26}$$

$$-K\frac{\mathrm{d}\phi_\mathrm{s}}{\mathrm{d}x} = j_\mathrm{s} \tag{27}$$

where j and j_s denote proton and electronic current density, respectively; ϕ_m and ϕ_s the electrical potential in the ionomer and carbon phase; and σ and x the corresponding effective conductivities.

The proton and electron current densities are related to the respective molar fluxes according to

$$\frac{\mathrm{d}j}{\mathrm{d}x} = -\frac{\mathrm{d}j_\mathrm{s}}{\mathrm{d}x} \tag{28}$$

Integrating over the catalyst layer gives

$$j + j_\mathrm{s} = j_\mathrm{l} \tag{29}$$

where j_l is the current density loading for the cell, noting that at $x = 0$, the membrane is electronically insulating, i.e. $j|_{x=0} = 0$ and thus $j_\mathrm{l} = j|_{x=0}$

In the catalyst region the over potential, η, driving reaction is defined as

$$\eta = -(\phi_\mathrm{s} - \phi_\mathrm{m}) \tag{30}$$

The change in over potential, from Eqs. (26) and (27), is

$$\frac{\mathrm{d}\eta}{\mathrm{d}x} = -\left(\frac{j}{\sigma} - \frac{j_\mathrm{s}}{K}\right) \tag{31}$$

Substituting Eq. (29) into (31) gives

$$\frac{\mathrm{d}\eta}{\mathrm{d}x} = -j\left[\frac{1}{K} + \frac{1}{\sigma}\right] + \frac{j_\mathrm{l}}{K} \tag{32}$$

In many cases e.g. for carbon supports, the electrical conductivity in the ionomer layer is much less than that in the carbon layer and the terms $1/K$ can be ignored in Eq. (32), except at low current densities. However other lower conductivity supports are being considered in certain fuel cell (e.g. conducting polymers) and thus we do not adopt this assumption.

3.1. Model solution

In the first instance we seek a solution to the current distribution problem assuming kinetics for the reaction given by Eq. (16). From this we will establish the overall electrode potential current density relationship for the electrode.

In the catalyst region, the change in ionic current density, i.e. due to proton conductivity is given by

$$\frac{\mathrm{d}j}{\mathrm{d}x} = -aj \tag{33}$$

where, a, is a specific reaction surface area (m^{-1}).

Differentiating Eq. (16) we obtain

$$\frac{\mathrm{d}j}{\mathrm{d}x} = \frac{\mathrm{d}\eta}{\mathrm{d}x}\left[\beta j - \frac{k_{20}}{6Fk_{10}}\beta j^2\right] \tag{34}$$

Combining Eqs. (33) and (34) we obtain

$$\begin{aligned}\frac{\mathrm{d}^2 j}{\mathrm{d}x^2} &= -a\frac{\mathrm{d}j}{\mathrm{d}x} = a\beta\left[j - \frac{k_{20}}{\hat{k}_{10}}j^2\right]\left[j\left(\frac{1}{K} + \frac{1}{\sigma}\right) - \frac{j_\ell}{K}\right] \\ &= a\beta\left(\frac{1}{K} + \frac{1}{\sigma}\right)\left(j^2 - \frac{k_{20}}{\hat{k}_{10}}j^3\right) - \frac{a\beta}{K}j_\ell\left[j - \frac{k_{20}}{\hat{k}_{10}}j^2\right], \\ \hat{k}_{10} &= 6Fk_{10}\end{aligned} \tag{35}$$

and hence

$$\begin{aligned}\frac{\mathrm{d}^2 j}{\mathrm{d}x^2} &= -\beta\left(\frac{1}{K} + \frac{1}{\sigma}\right)\frac{\mathrm{d}j}{\mathrm{d}x}\left(j - \frac{k_{20}}{k_{10}}j^2\right) \\ &\quad + \frac{\beta j_\ell}{K}\left[1 - \frac{k_{20}}{k_{10}}j\right]\frac{\mathrm{d}j}{\mathrm{d}x}\end{aligned} \tag{36}$$

We now introduce dimensionless variables

$$\text{let } z = \frac{x}{\ell}, \qquad j^* = \beta\ell\left(\frac{1}{K} + \frac{1}{\sigma}\right)j$$

and

$$\frac{\hat{k}_{10}}{k_{20}}\left(\beta\ell\left(\frac{1}{K} + \frac{1}{\sigma}\right)\right) = i^*, \qquad e = \frac{\beta\ell j_\ell}{K}$$

also

$$e = j_0^*\frac{1}{1 + (K/\sigma)}$$

Then Eq. (36) becomes

$$\frac{\mathrm{d}^2 j^*}{\mathrm{d}z^2} = -j^*\frac{\mathrm{d}j^*}{\mathrm{d}z} + \frac{j^{*2}}{i^*}\frac{\mathrm{d}j^*}{\mathrm{d}z} + e\left[1 - \frac{j^*}{i^*}\right]\frac{\mathrm{d}j^*}{\mathrm{d}z} \tag{37}$$

noting that $j^*\,\mathrm{d}j^* = (1/2)\,\mathrm{d}(j^*)^2$ gives

$$\frac{\mathrm{d}^2 j^*}{\mathrm{d}z^2} + \frac{1}{2}\frac{\mathrm{d}(j^*)^2}{\mathrm{d}z} - \frac{1}{3i^*}\frac{\mathrm{d}(j^*)^3}{\mathrm{d}z} - e\frac{\mathrm{d}j^*}{\mathrm{d}z} + \frac{e}{2i^*}\frac{\mathrm{d}j^{*2}}{\mathrm{d}z} = 0 \tag{38}$$

Integration gives

$$\begin{aligned}&\frac{\mathrm{d}j^*}{\mathrm{d}z} + \frac{j^{*2}}{2}\left(1 + \frac{e}{i^*}\right) - \frac{j^{*3}}{3i^*} - ej^* \\ &\quad = -J_0^* - \frac{j_0^{*3}}{3j_\mathrm{L}^*} - ej_0^* + \frac{j_0^{*2}}{2}\left(1 + \frac{e}{j_\mathrm{L}^*}\right) = \hat{J}\end{aligned} \tag{39}$$

with

$$j^* = \beta\ell\left(\frac{1}{K} + \frac{1}{\sigma}\right)j$$

and

$$J^* = -\left.\frac{\mathrm{d}j^*}{\mathrm{d}z}\right|_0 = a\ell j_\ell$$

where j_ℓ is the current density at the membrane catalyst interface which is a function of the electrode overpotential, i.e. $J^* = al6F(Ck_{10}\,e_0^{\beta\eta}/(1 + Ck_{20}\,e_0^{\beta\eta}))$

Re-arranging Eq. (39) gives the current distribution:

$$\frac{dj^*}{dz^2}\left[1 + \frac{e}{a\ell} + \frac{j^{*2}}{3a\ell i^*}\right] = \bar{J} - \frac{j^{*2}}{2}\left(1 + \frac{e}{i^*}\right) \quad (40)$$

Integration gives

$$\left(a + \frac{b\bar{J}}{d}\right)\left(\frac{1}{\sqrt{-\bar{J}d}}\tan^{-1}\left(\sqrt{\frac{-d}{\bar{J}}}j^*\right)\right) + \frac{bj^*}{d} = (1 - z),$$

$$a = \left(1 + \frac{e}{a\ell}\right),\ d = \frac{1}{2}\left(1 + \frac{e}{i^*}\right),\ b = \frac{1}{3a\ell i^*},\ c = \bar{J} \quad (41)$$

For $z = 0$ Eq. (41) becomes

$$j_0^* = \frac{1}{\sqrt{d/ - \hat{J}}}\tan\left[\frac{-(b/d)j_0^* + 1}{(1/\sqrt{-\hat{J}d})(\bar{a} + (b\hat{J}/d))}\right] \quad (42)$$

when $e = 0$, i.e. a high electronic conductivity catalyst layer equation (32) gives

$$j_0^* = \frac{1}{\sqrt{-1/2c}}\tan\left(\frac{1 - (2bj_0^*/1)}{(1 + (2bc/1))(1/\sqrt{-c/2})}\right)$$

3.2. Current distribution model for the Gasteiger mechanism

By following the same procedure as above for developing the current distribution model we can generate the differential equation defining the current distribution in the anode catalyst as

$$\frac{d^2j}{dx^2} = -a\frac{dj}{dx} = a\beta\left[j - \frac{k_{20}}{\hat{k}_{10}}j^2\right]\left[j\left(\frac{1}{K} + \frac{1}{\sigma}\right) - \frac{j_\ell}{K}\right]$$
$$= a\beta\left(\frac{1}{K} + \frac{1}{\sigma}\right)\left(j^2 - \frac{k_{20}}{\hat{k}_{10}}j^3\right) - \frac{a\beta}{K}j_\ell\left[j - \frac{k_{20}}{\hat{k}_{10}}j^2\right] \quad (25')$$

where

$$\hat{k}_{10} = 6FC_M k_{10}$$

Solution of this equation using similar procedures as above gives the current distribution as

$$j_0^* = \frac{1}{\sqrt{-d/c}}\tan\left(\frac{1 - (bj_0^*/d)}{(a + (bc/d))(1/\sqrt{-cd})}\right) \quad (32')$$

where

$$a = \left(1 + \frac{e}{a\ell}\right), \qquad d = \frac{1}{2}\left(1 + \frac{e}{i^*}\right),$$

$$b = \frac{1}{3a\ell i^*}, \qquad c = \bar{J}$$

4. Results of current distribution model

The treatment of the experimental data in Section 2 is based on an assumption that the electrode was pseudo-two-dimensional and was not porous. In practice the electrode was made as a Nafion bound carbon supported structure several microns in thickness and exhibits a current distribution normal to the flow of current. In this section, we investigate the simple current distribution model presented in Section 3 and its influence on the overall anode polarisation characteristics.

Fig. 9 shows typical dimensionless current density distribution in the anode catalyst. The behaviour reflects the expected decrease in local current density from the membrane surface into the electrocatalyst structure associated the gradual decrease in ionic current.

Fig. 10 shows typical dimensionless polarisation characteristics of the anode; i.e. dimensionless current density as a function of, J^*, the volumetric current density.

Fig. 11 shows the effect of methanol concentration on the overall anode polarisation characteristics for the Frelink

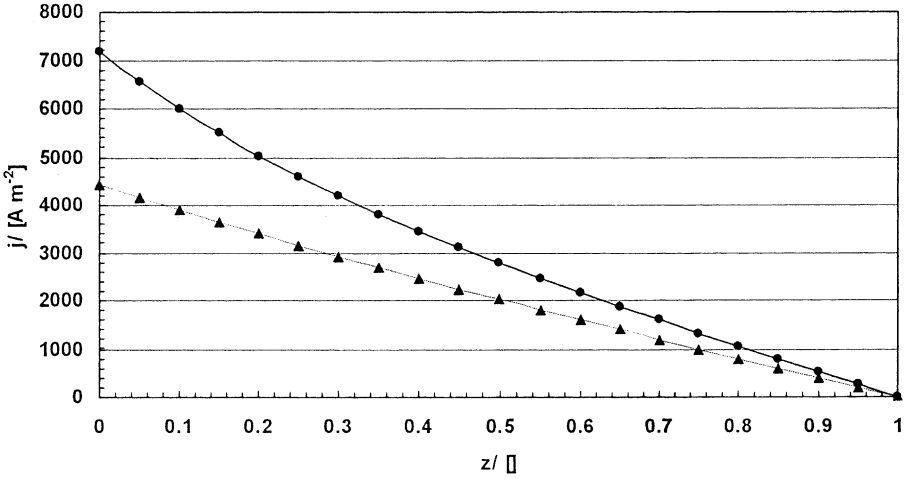

Fig. 9. Anode current density distribution: (●) $J^* = 15$, (▲) $J^* = 5$, $C_M = 1000\,\text{mol}\,\text{m}^{-3}$, $k_{10} = 8.64 \times 10^{-10}$, $\beta = 24.9$, $k_{20} = 5.83\text{E}{-}08$, $\alpha = 375$, $\ell = 1\text{E}{-}5$, $\sigma = 3.4$, $K = 40$.

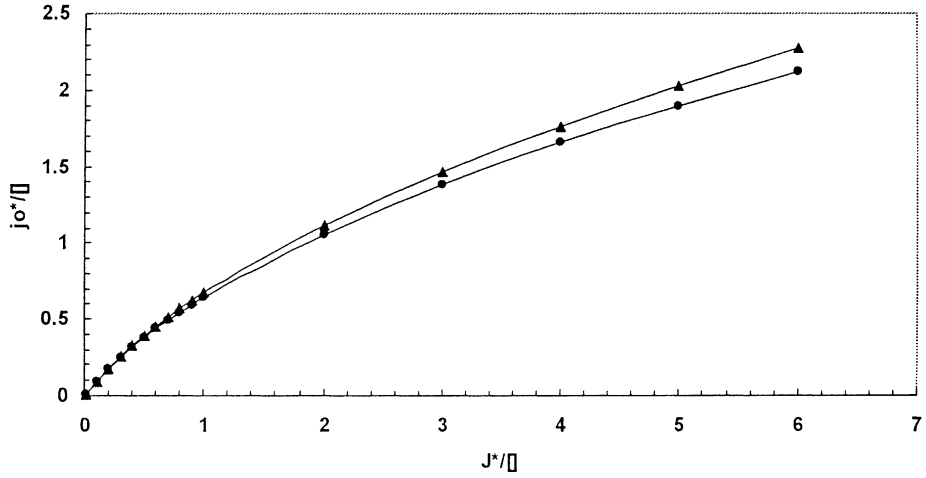

Fig. 10. Dimensionless anode polarisation behaviour: (▲) $K = 40$, (●) $K = 4000$, $\alpha = 130\,000$, $\ell = 1\text{E}{-5}$, $\sigma = 3.4$. $k_{10} = 1.22\text{E}{-05}$, $\beta = 17.91819$, $k_{20} = 0.768343$.

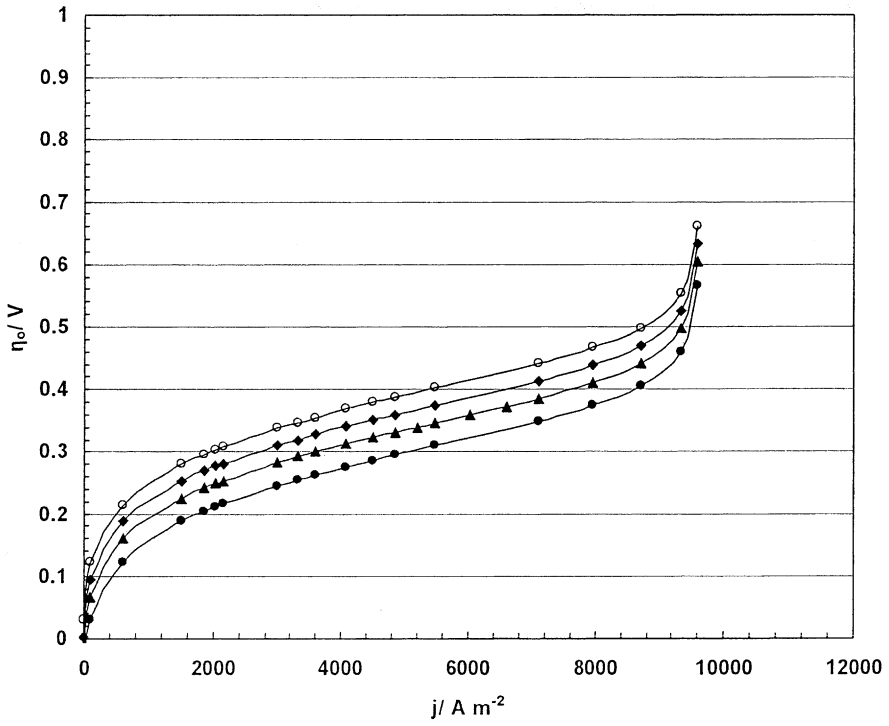

Fig. 11. The effect of methanol concentration on anode polarisation characteristics: $k_{10} = 8.64\text{E}{-10}$, $\beta = 24.90$, $k_{20} = 5.83\text{E}{-08}$, $\alpha = 375$, $\ell = 1\text{E}{-5}$, $\sigma = 3.4$, $K = 40$. (◆) $C_M = 2500$, (●) $C_M = 500$, (▲) $C_M = 1000$, (○) $C_M = 250$.

model (Eq. (16)). The values of parameters selected (thickness, conductivity) are those that are in general accord with the actual fuel cell anode although the exact values are not known. The model generally gives reasonable agreement with experimental data by adjusting the parameter k_{10}. The values of the parameter k_{10} are much lower than those used to model data, for a pseudo-two-dimensional electrode, in Section 2 and is essentially due to the much higher surface area for oxidation in the porous electrocatalyst. The data show that increasing methanol concentration reduces the extent of anode polarisation and that regardless of the methanol concentration one "limiting" current density is approached. The behaviour at low polarisation is approximately in agreement of observations that the methanol oxidation is a half order reaction in methanol concentration, i.e. at a fixed overpotential, an order of magnitude increase in concentration produces an approximate 3 to 4 increase in current.

Fig. 12 shows the effect of methanol concentration on the overall anode polarisation characteristics for the Gasteiger model (32). This model with appropriate parameters gives polarisation behaviour that is in accord with experimental data. The model exhibits the trends that at low current den-

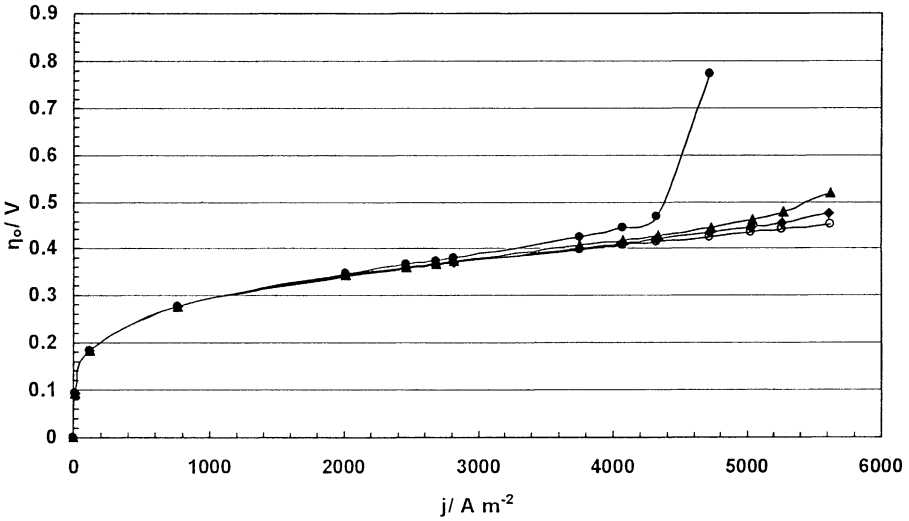

Fig. 12. The effect of methanol concentration on anode polarisation characteristics. $k_{10} = 8.46\text{E}{-10}$, $\beta = 24.90$, $k_{20} = 5.83\text{E}{-8}$, $\alpha = 375$, $\ell = 1\text{E}{-5}$, $\sigma = 3.4$, $K = 40$. (○) $C_M = 2500$, (◆) $C_M = 1500$, (●) $C_M = 500$, (▲) $C_M = 1000$.

sities the anode polarisation does not vary with methanol concentration and that at higher anode polarisation limiting current densities are approached which depend upon the concentration of methanol. The former observation is not consistent with reported data for methanol oxidation by a number of researchers [2,7].

5. Conclusions

A model of the current distribution in a methanol oxidation fuel cell anode is presented which can be used in conjunction with a kinetic model of the oxidation to predict anode fuel cell polarisation behaviour. The ability of the model to accurately predict the polarisation behaviour relies on the availability of accurate parameters for the anode structure and the kinetic parameters. In addition the suitability of the model requires confirmation of the mechanism for methanol oxidation, albeit an approximation, so that a suitable kinetic equation can be used. The latter equation should be in agreement with the effect of methanol concentration on the kinetics and mass transfer characteristics during oxidation. The latter aspect is the subject of ongoing work in the laboratories at Newcastle.

Acknowledgements

The authors would like to acknowledge the following:

The European Commission for a TMR Marie Curie B20 and an IHP Marie Curie B30 research training grant to Dr. P. Argyropoulos.

The work was performed in research facilities provided through an EPSRC/HEFCE Joint Infrastructure Fund award no. JIF4NESCEQ.

References

[1] G.L. Troughton, A. Hamnett, Bull. Electrochem. 7 (1991) 488.
[2] P.S. Kaurenan, E. Skou, J. Electroanal. Chem. 408 (1996) 189.
[3] D. Chu, S. Gilman, J. Electrochem. Soc. 141 (1994) 1770.
[4] K. Scott, W.M. Taama, J. Cruickshank, J. Power Sources 65 (1997) 159.
[5] J.S. Wainwright, J.T. Weng, R.F. Savinell, M. Litt, J. Electrochem. Soc. 142 (1995) L121.
[6] Direct Methanol Fuel Cell Review Meeting, Department of Energy and Advanced Research Projects Agency, Baltimore, April 26–27, 1994.
[7] M.K. Ravikumar, A.K. Shukla, J. Electrochem. Soc. 143 (1996) 2601.
[8] S. Surampudi, S.R. Narayanan, E. Vamos, H. Frank, G. Halpert, A. LaConti, J. Kosek, G.K. SuryanPakash, G.A. Olah, J. Power Sources 47 (1994) 377.
[9] T.I. Valdez, S.R. Narayanan, H. Frank, W. Chun, Proceedings of the 12th Annual Battery Conference on Applications and Advances, 1997, p. 239.
[10] S.R. Narayana, G. Halpert, W. Chun, B. Jeffries-Nakamura, T.I. Valdez, H. Frank, S. Surampudi, Proceedings of the Power Sources Conference, Cherry Hill, NJ, USA, 1996.
[11] B. Prater, J. Power Sources 51 (1994) 129.
[12] M. Hogarth, P. Christensen, A. Hamnett, A.K. Shukla, J. Power Sources 55 (1995) 87.
[13] K. Scott, W.M. Taama, P. Argyropoulos, J. Appl. Electrochem. 28 (1998) 1389.
[14] X. Ren, W. Henderson, S. Gottesfeld, J. Electrochem. Soc. 144 (9) (1997) L267.
[15] M.W. Verbrugge, J. Electrochem. Soc. 136 (1989) 417.
[16] J. Cruickshank, K. Scott, J. Power Sources 70 (1998) 40.
[17] K. Scott, J. Cruickshank, J. Appl. Electrochem. 28 (1998) 289.
[18] S.F. Baxter, V.S. Battaglia, R.E. White, J. Electrochem. Soc. 146 (1999) 437.
[19] A.A. Kulikovsky, J. Divisek, A.A. Kornyshev, J. Electrochem. Soc. 147 (2000) 953.
[20] A.A. Kulikovsky, J. Appl. Electrochem. 30 (2000) 1005.
[21] K. Sundmacher, T. Schultz, S. Zhou, K. Scott, M. Ginkel, E.D. Gilles, Chem. Eng. Sci. 56 (2001) 333.
[22] Z.H. Wang, C.Y. Wang, in: S.R. Narayanan, S. Gottesfeld, T. Zawodzinski (Eds.), Direct Methanol Fuel Cells, Proceedings of the

International Symposium, The Electrochemical Society, NJ, 2001, p. 286.
[23] C.Y. Wang, K.S. Chen, Adv. Heat Transfer 30 (2001) 40.
[24] J.P. Meyers, J. Newman, J. Electrochem. Soc. 149 (2002) A718.
[25] J.P. Meyers, J. Newman, J. Electrochem. Soc. 149 (2002) A710.
[26] H.A. Gaisteiger, N. Markovic, P.N. Ross Jr., P.N.J. Cairns, J. Phys. Chem. 97 (1993) 12020.
[27] T. Frelink, W. Visscher, J.A.R. van Veen, Langmuir 12 (1996) 3702.
[28] A.K. Shukla, K. Scott, C.L. Jackson, R.K. Raman, Electrochim. Acta 47 (2002) 3401.
[29] K. Scott, W.M. Taama, P. Argyropoulos, K. Sundmacher, J. Power Sources 83 (1999) 204.
[30] K. Scott R. Allen, C. Lim, S. Roy, Electrochim. Acta, in press.